

Secrecy Rate Maximization for Reconfigurable Intelligent Surface Aided Millimeter Wave System with Low-resolution DAC

Yue Xiu, Jun Zhao, Zhongpei Zhang

Abstract—In this letter, we investigate the secrecy rate of a reconfigurable intelligent surface (RIS)-aided millimeter-wave (mmWave) system with hardware limitations. Compared to the RIS-aided systems in most existing works, we consider the case of the RIS-aided mmWave system with low-resolution digital-to-analog converters (LDACs). We formulate a secrecy rate maximization problem hardware constraints. Then by optimizing the RIS phase shift and the transmit beamforming to maximize the secrecy rate. Due to the nonconvexity of the problem, the formulated problem is intractable. To handle the problem, an alternating optimization (AO)-based algorithm is proposed. Specifically, we first use the successive convex approximation (SCA) method to obtain the transmit beamforming. Then the element-wise block coordinate descent (BCD) method is used to obtain the RIS phase shift. Numerical results demonstrate that the RIS can mitigate the hardware loss, and the proposed AO-based algorithm with low complexity outperforms the baselines.

Index Terms—Reconfigurable intelligent surface, millimeter-wave, low-resolution digital-to-analog converter, alternating optimization algorithm.

I. INTRODUCTION

Millimeter-wave (mmWave) technologies have played an important role in 5G communication systems. Compared to the microwave, the mmWave can achieve large system capacity and security performance [1]. However, the blockage issue needs to be tackled before the commercial application of this technology. Specifically, mmWave frequencies are susceptible to the blockage, which means mmWave communications are difficult to be applied in urban areas with dense buildings [2].

To handle this problem, reconfigurable intelligent surface (RIS) is proposed as a promising technology to provide more propagation paths for mmWave communication systems [10]. In particular, by adjusting the reflection matrix of RIS, the propagation direction of the transmitted signal can be changed. Moreover, since RIS can significantly improve the beamforming gain, the RIS can extend the coverage of mmWave communication systems as well [1], [2], [11].

Recently, the secure problem of RIS-aided mmWave systems has been investigated in [7]–[9]. Specifically, in [7], the authors maximized the secrecy rate of RIS-aided communication systems by optimizing the RIS phase shift and the transmit beamforming. In [8], the sum secrecy rate maximization for multi-user mmWave systems was studied, and a low-complexity iterative algorithm was proposed for the RIS-aided mmWave system. In [9], by jointly optimizing hybrid precoding at APs and phase shifting at the RIS to maximize the secrecy rate for RIS-aided mmWave systems.

However, the RIS-aided mmWave security systems with hardware limitations have not been investigated yet. In general, compared with the low-resolution digital-to-analog converters (LDACs) at the access point (AP), much more power consumption is needed for the high-resolution DACs [12]. Hence, to cut the hardware cost and power budget, LDACs have been widely used in the mmWave system. In addition to the hardware imperfections due to LDACs, IRS phase noise,

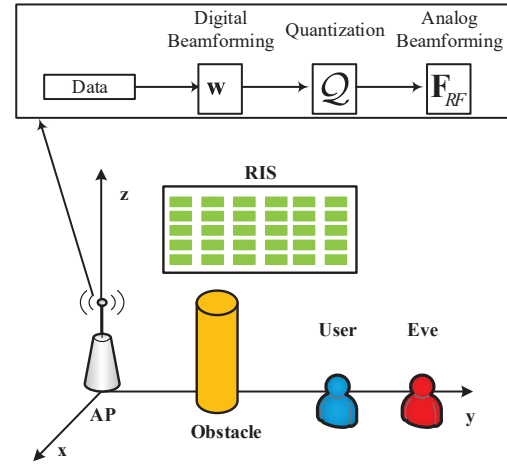


Fig. 1: An RIS-aided mmWave secure communication system with hardware limitations.

caused by finite discrete phase shifts of the IRS, is another crucial hardware impairment in IRS-aided systems [6], [14]. Hence, to degrade the hardware loss from transmitter and RIS, we consider the RIS-aided mmWave system with hardware limitations.

To the best of our knowledge, the existing works in [1]–[6], [10] do not consider the downlink RIS-aided mmWave communication system with hardware limitations. Therefore, it is meaningful to study the impact of the hardware limitations in the RIS-aided mmWave communication system. Motivated by this, we focus on an RIS-aided mmWave security system with LDACs and phase noise from RIS. Specifically, we maximize the secrecy rate under these hardware constraints by jointly optimizing the transmit beamforming and the RIS phase shift. Since the objective function and the feasible set are non-convex, the formulated problem is intractable. To cope with these difficulties, we propose an alternating optimization (AO)-based algorithm. Specifically, we first apply the successive convex approximation (SCA) method to recast this problem into a tractable optimization problem and obtain the transmit beamforming matrix. Then, we propose an element-wise block coordinate descent (BCD) method to obtain the RIS phase shift, respectively. Our results reveal that by optimizing the transmit beamforming and the phase shift of RIS, the hardware loss can be mitigated and improve the secrecy rate of the RIS-aided mmWave system.

II. SYSTEM MODEL

We consider an RIS-aided massive MIMO mmWave downlink, as shown in Fig. 1, where the AP is equipped with N_t antennas and N_{RF} RF chains sends data to the user and eavesdropper (Eve). The user and Eve are equipped with a single antenna, respectively. Considering N_t being typically large, we assume a hybrid beamforming at the AP with 1-bit DACs to degrade the complexity and infinite-resolution

ADCs at the user and Eve, due to relatively smaller single antenna. Moreover, the RIS is equipped with N_r reflection elements. In this paper, we adopt a geometric model for mmWave channels [10]. $\mathbf{G} \in \mathbb{C}^{N_r \times N_t}$ denotes the AP-to-RIS mmWave channel. $\mathbf{F}_{RF} \in \mathbb{C}^{N_t \times N_{RF}}$ and $\mathbf{w} \in \mathbb{C}^{N_{RF} \times 1}$ are the analog beamforming codebook and digital beamforming vector, respectively. \mathbf{F}_{RF} adopt the semi-unitary codebook [13]. $\mathcal{Q}(\cdot)$ denotes the 1-bit quantizer.

We assume the RIS phase shift as $\Theta = \text{diag}(\boldsymbol{\theta}) \in \mathbb{C}^{N_r \times N_r}$, where $\boldsymbol{\theta} = [\beta e^{j\phi_1}, \dots, \beta e^{j\phi_{N_r}}] \in \mathbb{C}^{1 \times N_r}$. $\phi_i \in [0, 2\pi]$, $\forall i = 1, \dots, N_r$ and $\beta = 1$ denote the phase shift and the amplitude reflection coefficient with the passive element of the RIS, respectively. According to [16], due to the hardware limitation, the RIS can only choose its phase shifts from a finite number of discrete values. Specifically, ϕ_i can only be chosen from a finite set of discrete values $\mathcal{G} = \{0, \Delta\theta, \dots, (L-1)\Delta\theta\}$, L is the number of discrete values, and $\Delta\theta = \frac{2\pi}{L}$. Due to unfavorable propagation conditions (obstacles, buildings), the direct links from the AP to the users are ignored. Then, the RIS reflects the signal to the user and Eve, and the received signal at the user and Eve can be expressed as

$$y = \mathbf{h}^H \Theta \mathbf{G} \mathbf{F}_{RF} \mathcal{Q}(\mathbf{w}s) + n, \quad (1)$$

and

$$y_e = \mathbf{h}_e^H \Theta \mathbf{G} \mathbf{F}_{RF} \mathcal{Q}(\mathbf{w}s) + n_e, \quad (2)$$

in which $n \sim \mathcal{CN}(0, \sigma^2)$ and $n_e \sim \mathcal{CN}(0, \sigma_e^2)$ are the additive white Gaussian noise. $\mathbf{h} \in \mathbb{C}^{N_r \times 1}$ and $\mathbf{h}_e \in \mathbb{C}^{N_r \times 1}$ are the channel matrix between the RIS and the user, Eve, respectively.

III. LINEAR QUANTIZATION MODELS

We consider the linear additive quantization noise model (AQNM) schemes [17] for the non-linear quantization operator $\mathcal{Q}(\cdot)$. The AQNM scheme is widely adopted thanks to its simplicity. The respective linearization is expressed as follows

$$\mathcal{Q}(\mathbf{w}s) \approx \mathbf{B}_Q \mathbf{w}s + \mathbf{q}_Q, \quad (3)$$

where \mathbf{B}_Q is the weight matrix and it is expressed as

$$\mathbf{B}_Q = \sqrt{1 - \eta_b} \mathbf{I}_{N_s}, \quad (4)$$

where η_b is the distortion factor, which is generally approximated by $\eta_b = \frac{\pi\sqrt{3}}{2} 2^{-2b}$ for b -bit quantization with sufficiently large b , while its more accurate value for 1-bit quantization is $\eta_b \approx 0.3634$ [17]. In (3), \mathbf{q}_Q stands for the quantization distortion with the following covariance

$$\mathbf{A}_Q = \frac{P}{N_s} \eta_b (1 - \eta_b) \text{diag}(\mathbf{w}\mathbf{w}^H). \quad (5)$$

Then the achievable rate at the user can be expressed as

$$R = \log_2 \left(1 + \frac{|\sqrt{1 - \eta_b} \mathbf{h}^H \Theta \mathbf{G} \mathbf{F}_{RF} \mathbf{w}|^2}{\|\mathbf{h}^H \Theta \mathbf{G} \mathbf{F}_{RF} \mathbf{A}_Q \text{diag}(\mathbf{w})\|^2 + \sigma^2} \right). \quad (6)$$

The achievable rate at the user can be expressed as

$$R_e = \log_2 \left(1 + \frac{|\sqrt{1 - \eta_b} \mathbf{h}_e^H \Theta \mathbf{G} \mathbf{F}_{RF} \mathbf{w}|^2}{\|\mathbf{h}_e^H \Theta \mathbf{G} \mathbf{F}_{RF} \mathbf{A}_Q \text{diag}(\mathbf{w})\|^2 + \sigma_e^2} \right). \quad (7)$$

The system secrecy rate can be written as

$$R_s = [R - R_e]^+, \quad (8)$$

where $[x]^+ = \max(0, x)$. Then by optimizing the RIS phase shift and the transmit beamforming to maximize the system secrecy rate, and the problem is formulated as

$$\max_{\Theta, \mathbf{w}} R_s \quad (9a)$$

$$\text{s.t. } |\phi_i| = 1, \phi_i \in \mathcal{G} \quad (9b)$$

$$\|\mathbf{F}_{RF} \mathcal{Q}(\mathbf{w}s)\|^2 \leq P, \quad (9c)$$

where (9c) is the power constraint, and P is the maximum transmit power. (9b) denotes the unit-modulus constraint. Incorporating (9c) and (5), and the fact that data and quantization

noise is independent of the transmitted data, the transmit power constraint is rewritten as

$$\begin{aligned} \|\mathbf{F}_{RF} \mathcal{Q}(\mathbf{w}s)\|^2 &= \frac{P}{N_s} \|\sqrt{1 - \eta_b} \mathbf{F}_{RF} \mathbf{w}\|^2 + \text{tr}(\mathbf{F}_{RF} \mathbf{A}_Q \mathbf{F}_{RF}) \\ &= \frac{P}{N_s} \|\sqrt{1 - \eta_b} \mathbf{w}\|^2 + \text{tr}(\mathbf{A}_Q), \end{aligned} \quad (10)$$

which follows from the semi-unitary \mathbf{F}_{RF} . Therefore, problem (9) is rewritten as

$$\max_{\Theta, \mathbf{w}} R_s \quad (11a)$$

$$\text{s.t. (9b),} \quad (11b)$$

$$\frac{P}{N_s} \|\mathbf{A}_Q \mathbf{w}\|^2 + \text{tr}(\mathbf{B}) \leq P. \quad (11c)$$

IV. ALTERNATING OPTIMIZATION ALGORITHM

We adopt alternating-optimization (AO)-based algorithm to optimize \mathbf{w} and Θ separately, rather than solving (11) for \mathbf{w} and Θ jointly which is computationally far too expensive.

A. Digital Beamforming Optimization

Under given Θ , problem (11) is rewritten as

$$\max_{\mathbf{w}} \log_2 \left(1 + \frac{|\mathbf{D}\mathbf{w}|^2}{\omega} \right) - \log_2 \left(1 + \frac{|\mathbf{D}_e \mathbf{w}|^2}{\omega_e} \right) \quad (12a)$$

$$\text{s.t. (11c),} \quad (12b)$$

where

$$\mathbf{D} = \sqrt{1 - \eta_b} \mathbf{h}^H \Theta \mathbf{G} \mathbf{F}_{RF}, \mathbf{D}_e = \sqrt{1 - \eta_b} \mathbf{h}_e^H \Theta \mathbf{G} \mathbf{F}_{RF},$$

$$\omega = |\mathbf{h}^H \Theta \mathbf{G} \mathbf{F}_{RF} \mathbf{A}_Q \text{diag}(\mathbf{w})|^2 + \sigma^2,$$

$$\omega_e = |\mathbf{h}_e^H \Theta \mathbf{G} \mathbf{F}_{RF} \mathbf{A}_Q \text{diag}(\mathbf{w})|^2 + \sigma_e^2. \quad (13)$$

Then, to deal with the non-convex objective function in (12a), we use auxiliary variable t to rewrite (12) as

$$\max_{\mathbf{w}} \log_2 \left(1 + \frac{|\mathbf{D}\mathbf{w}|^2}{\omega} \right) - t \quad (14a)$$

$$\text{s.t. (11c),} \quad (14b)$$

$$t = \log_2 \left(1 + \frac{|\mathbf{D}_e \mathbf{w}|^2}{\omega_e} \right). \quad (14c)$$

It is not difficult to find that the objective function is still non-convex. To handle the non-convex objective function, we use ρ to further transform (14a) as

$$\log_2(1 + \rho) - t, \quad (15)$$

where

$$\rho \leq \frac{|\mathbf{D}\mathbf{w}|^2}{\omega}. \quad (16)$$

According to Schur complement [15], we have

$$\begin{bmatrix} 1 & z \\ z & |\mathbf{D}\mathbf{w}|^2 \end{bmatrix} \succeq \mathbf{0}, \rho \leq \frac{z^2}{\omega}. \quad (17)$$

Then, we use the SCA method based on the first-order Taylor expansion [3] to tackle $\rho \geq \frac{z^2}{\omega}$. Specifically, $\rho \geq \frac{z^2}{\omega}$ is non-convex with respect to ρ and ω , and thus it can be tightly bounded from below with its first-order approximation. In particular, for any fixed points $(\bar{z}, \bar{\omega})$, we have

$$\frac{z^2}{\omega} \geq \frac{2\bar{z}}{\bar{\omega}} z - \frac{\bar{z}^2}{\bar{\omega}^2} \omega \geq \rho. \quad (18)$$

By applying the concept of SCA [3], [4], we iteratively update \bar{t}_k and $\bar{\omega}_k$ in the n -th iteration as

$$\bar{\omega}^{(n)} = \omega^{(n-1)}, \bar{z}^{(n)} = z^{(n-1)}. \quad (19)$$

Now, we handle the non-convex constraint in (14c), similarly, we use Schur complement to deal with (14c) and (14c) can be transformed into the following equivalent form

$$\begin{bmatrix} 2^t - 1 & r \\ r & \omega \end{bmatrix} \succeq \mathbf{0}, \quad (20)$$

$$r^2 \leq (2^t - 1)\omega, \quad (21)$$

and

$$r^2 - |\mathbf{D}\mathbf{w}|^2 = 0. \quad (22)$$

In order to deal with the bilinear function on the left-hand side of (21), the SCA method based on the arithmetic geometric mean (AGM) inequality is adopted, so (21) can be rewritten as

$$\frac{1}{2} \left((\omega\eta)^2 + \left(\frac{2^t-1}{\eta} \right)^2 \right) - \bar{r}(r - \bar{r}) \geq 0, \quad (23)$$

where η is a feasible point. To tighten the upper bound, η is iteratively updated. The update formulation in the n -th iteration is expressed as

$$\eta^{(n)} = \sqrt{\frac{2^{t(n-1)}-1}{\rho^{(n-1)}}}. \quad (24)$$

Then, we deal with non-convex constraint (22) and use the SCA method to transform (22) as the following convex constraints

$$\begin{aligned} |\mathbf{D}\mathbf{w}|^2 - \bar{r}(r - \bar{r}) &\geq 0, \\ r^2 - |\mathbf{D}\bar{\mathbf{w}}|^2 - 2\text{Re}(\bar{\mathbf{w}}^H \mathbf{D}^H \mathbf{D}(\mathbf{w} - \bar{\mathbf{w}})) &\geq 0. \end{aligned} \quad (25)$$

The non-convex constraint in (11c) can be rewritten as the following form by using an similar manner with (25)

$$\frac{P}{N_s} (|\sqrt{1-\eta_b}\bar{\mathbf{w}}|^2 - 2\text{Re}((1-\eta_b)\bar{\mathbf{w}}^H(\mathbf{w} - \bar{\mathbf{w}}))) + \text{tr}(\mathbf{A}_Q) \leq P. \quad (26)$$

Now, the problem in (12) is transformed the following convex approximation problem

$$\max_{t, r, \omega, \rho, z, \mathbf{w}} \log_2(1 + \rho) - t \quad (27a)$$

$$\text{s.t. (17), (18), (20), (23), (25), (26).} \quad (27b)$$

The SCA-based algorithm is summarize in **Algorithm 1** for (12). Due to the monotonic increasing of objective function (27a) in each iteration, the SCA-based algorithm can converge to a stable point.

Algorithm 1: SCA-based algorithm for problem (12).

- 1 **Initialization:** \bar{r} , $\bar{\omega}$, \bar{z} , $\bar{\mathbf{w}}$.
 - 2 **Repeat**
 - 3 Update $\{\mathbf{w}^{(n)}, r^{(n)}, \rho^{(n)}, \omega^{(n)}, z^{(n)}, t^{(n)}\}$ with fixed \bar{r} , $\bar{\omega}$, \bar{t} , $\bar{\mathbf{w}}$ by solving (27).
 - 4 Update $\eta^{(n+1)}$, $\bar{\omega}^{(n+1)}$, $\bar{z}^{(n+1)}$ based on (19) and (24).
 - 5 Update $n = n + 1$.
 - 6 **Until** Convergence.
 - 7 **Output:** \mathbf{w}^* .
-

B. Discrete RIS Phase Shift Optimization

Substituting the transmit beamforming vector \mathbf{w} obtained in previous section into problem (11). Then the sub-problem of phase shift matrix can be rewritten at the top of next page.

Since the variable ϕ_i belongs to a finite number of values, problem (28) can be resolved by using the exhaustive search method. However, feasible set \mathcal{G} is large and the complexity of exhaustive search method is very high. To reduce complexity, an element-wise BCD algorithm is proposed.

To obtain the closed form solution of phase shift, we employ the element-wise BCD method [3] to solve this problem. We assume ϕ_i as one block in the BCD and iteratively derive the continuous solutions of ϕ_i by using **Theorem 1**.

Theorem 1. *There exists solution ϕ_i^* to maximize the value of (28) by solving the following equation*

$$\begin{aligned} &\frac{(\mu_i - \bar{\mu}_i)t - \bar{\mu}_i}{\mu_i(1+t^2) + \bar{\mu}_i(1-t^2) - \bar{\mu}_i 2t} - \frac{(\eta_i - \bar{\eta}_i)t - \bar{\eta}_i}{\eta_i(1+t^2) + \bar{\eta}_i(1-t^2) - \bar{\eta}_i 2t} \\ &+ \frac{(\lambda_i - \bar{\lambda}_i)t - \bar{\lambda}_i}{\lambda_i(1+t^2) + \bar{\lambda}_i(1-t^2) - \bar{\lambda}_i 2t} - \frac{(\rho_i - \bar{\rho}_i)t - \bar{\rho}_i}{\rho_i(1+t^2) + \bar{\rho}_i(1-t^2) - \bar{\rho}_i 2t} = 0, \end{aligned} \quad (29)$$

We use one dimension search method in [19] to solve the equation in (29). ϕ_i^* can be expressed as

$$\phi_i^* = 2 \arctan(t). \quad (30)$$

The proof is given in Appendix A

According to **Theorem 1**, the discrete solution $\bar{\phi}_i^*$ can be calculate by the following formulation

$$\bar{\phi}_i^* = \arg \min_{\phi_i \in \mathcal{G}} |\phi_i^* - \phi_i|. \quad (31)$$

The algorithm based on element BCD can be summarized as **Algorithm 2**. Since the monotonically increasing of (28) in each iteration, the proposed can converge to a stable point.

Algorithm 2: Element-wise BCD-based algorithm for Problem (28).

- 1 **Initialization:** $t = 0$, Θ^0 .
 - 2 **Repeat:**
 - 3 **for:** $i = 1, \dots, N_r$
 - 4 Calculate ϕ_i^t based on **Theorem 1**.
 - 5 **End:**
 - 6 Set $t = t + 1$
 - 7 **Until:** Convergence.
 - 8 **Output:** the solution Θ^*
-

Based on the above analysis, we can obtain the AO-based algorithm for solving problem (9). Following the results in [3], since each sub-algorithm converges to a local optimal solution, we can guarantee that the AO-based algorithm can converge to a local optimal solution. .

Algorithm 3: AO-based Algorithm for problem (9).

- 1 **Initialization:** $\mathbf{w}^{(0)}$, $\Theta^{(0)}$.
 - 2 **Repeat**
 - 3 Update $\mathbf{w}^{(j)}$ by using **Algorithm 1**.
 - 4 Update $\Theta^{(j)}$ by using **Algorithm 2**.
 - 5 Update $j = j + 1$.
 - 6 **Until** Convergence.
 - 7 **Output:** \mathbf{w}^* , Θ^* .
-

C. Complexity analysis

The total complexity of the SDP-based method is about $\mathcal{O}(\zeta N_r^8 + N_t^2)$ [18], which mainly depends on the complexity of solving the SDP problem and the number of rank 1 solutions that construct the feasible set of the Gaussian randomization method ‘ ζ ’. The complexity of the proposed method is about $\mathcal{O}(N_r(N_r N_t + L_P) + N_t^2)$, which depends on the computational complexity of ϕ_i and \mathbf{w} calculation. Intuitively, these methods have lower complexity than the exhaustive method $\mathcal{O}(N_r^{L_P+1} + N_r^2 + N_r N_t)$, and the AO-based algorithm has the lowest complexity.

V. NUMERICAL RESULTS

As shown in Fig.1, we consider an RIS-aided mmWave system with hardware limitations, where AP’s coordinate is (0, 0, 0) and IRS is located at (0, 60, 20) m. While the user and the Eve are located at (5, 60, 0) m and (5, 80, 0) m, respectively. We set $N_t = 64$, $N_r = 16$, $M = 8$, $b = 1$, $\sigma^2 = -110$ dBm. The mmWave channels from the AP to the RIS, the RIS to the k th user are respectively expressed as

$$\mathbf{G} = \sqrt{\frac{1}{\beta_{L1}}} \sum_{l=0}^{L1-1} \alpha \mathbf{a}_T(N_T, \theta) \mathbf{a}_R^T(N_r, \varphi, \phi), \quad (32)$$

$$\mathbf{h}_k = \sqrt{\frac{1}{\beta_{kLk}}} \sum_{l=0}^{Lk-1} \hat{\alpha}_k \mathbf{a}_R(N_r, \vartheta_k), \quad k \in \{\text{user}, \text{Eve}\} \quad (33)$$

$$\max_{\Theta} \left(\frac{\|\theta^T \text{diag}(h^H) G F_{RF} A_Q \text{diag}(w)\|^2 + \sigma^2 + |\sqrt{1-\eta_b} h^H \Theta G F_{RF} w|^2}{\|\theta^T \text{diag}(h^H) G F_{RF} A_Q \text{diag}(w)\|^2 + \sigma^2} \right) \quad (28a)$$

$$\left(\frac{\|\theta^T \text{diag}(h_e^H) G F_{RF} A_Q \text{diag}(w)\|^2 + \sigma^2 + |\sqrt{1-\eta_b} h_e^H \Theta G F_{RF} w|^2}{\|\theta^T \text{diag}(h_e^H) G F_{RF} A_Q \text{diag}(w)\|^2 + \sigma^2} \right) \quad (28b)$$

$$\text{s.t. (9b)}$$

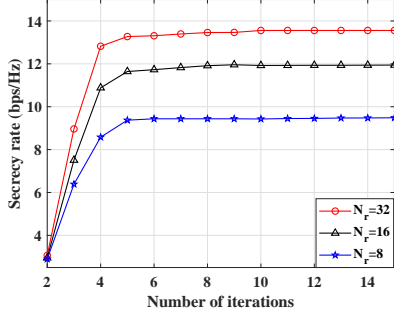


Fig. 3: Convergence of **Algorithm 3**

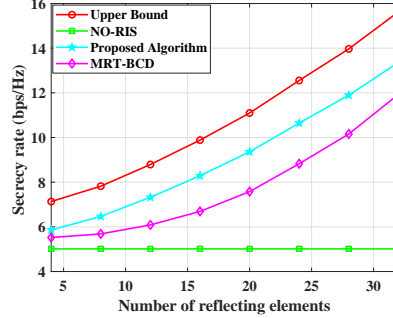


Fig. 4: Secrecy rate versus N_r

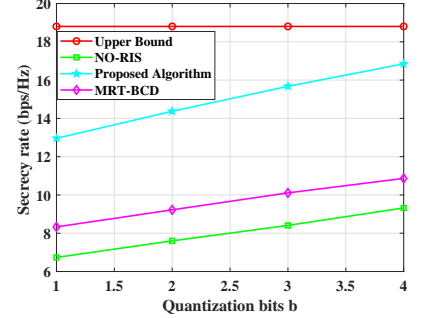


Fig. 5: Secrecy rate versus b

where β and $\hat{\beta}_k$ denote the large-scale fading coefficients. They are generated by

$$72 + 29.2 \log_{10} d + \zeta \quad (34)$$

where d denotes the signal propagation distance, $\zeta \sim \mathcal{CN}(0, 1)$ is the log-normal shadowing, α and $\hat{\alpha}_k$ denote the small-scale fading coefficients which follow $\mathcal{CN}(0, 1)$ [15]. $\mathbf{a}_T(\cdot)$ and $\mathbf{a}_R(\cdot)$ represent array steering vectors at the AP and the RIS, respectively. The following three schemes with fixed quantization bits for each DAC are also considered for comparison:

- **MRT-BCD**: In this scheme, the transmit beamforming is designed based on maximum ratio transmission (MRT). Then, the RIS phase shift is obtained by using **Algorithm 2**.
- **NO-RIS**: In this scheme, the mmWave do not use the RIS to assist communication. Moreover, the transmit beamforming is optimized by using **Algorithm 1**.
- **Upper Bound**: In this scheme, we consider the RIS-aided mmWave system without hardware limitations as the upper bound of performance. Moreover, the transmit beamforming matrix and the RIS phase shift are optimized by using **Algorithm 1** and **Algorithm 2** in this paper, respectively.

In Fig.2, we study the convergence behavior of the proposed AO-based algorithm under different iteration times. We observe that the secrecy rate increases monotonically with the increase of the number of iterations. In addition, the algorithm converges quickly, and generally only 5 iterations can achieve a high security rate. This shows that the proposed algorithm has low complexity.

Fig.3 shows the secrecy rate under different number of reflecting elements of the RIS. As expected, compared with the MRT-BCD and NO-RIS schemes, the proposed AO-based algorithm can achieve the best secrecy rate. From Fig.3, we also can see that the secrecy rate monotonically increases with the number of reflecting elements. This is because large numbers of reflecting elements can lead to high signal gain and suppress the Eve, which results in high secrecy rate of the system. Moreover, although the resolution of DAC is higher than that of the proposed scheme in upper bound scheme, we find that as the number of reflecting elements of RIS increases, both the proposed scheme and the upper bound scheme increase at the same time. This finding validates the

feasibility of using RIS to mitigate the influence of hardware limitations.

Fig.4 depicts the secrecy rate versus quantization bit for different schemes. We find that the secrecy rate of system achieved by the MRT-BCD scheme and NO-RIS scheme, and the proposed AO-based algorithm achieve the best performance in these schemes. Meanwhile, the average secrecy rate of proposed AO-based scheme significantly increases, but that of the MRT-BCD scheme increase slowly. This is due to the fact that the MRT-based algorithm aims to maximize the achievable rate of the user while ignoring the Eve and hardware limitations, which results in significant information leakage, while the proposed AO-based scheme can effectively prevent eavesdropping. It is not difficult to find that the schemes with the RIS can outperform the NO-RIS scheme. From the perspective of maximizing the secrecy rate, when the system is assisted by RIS, there is no need to deploy high-resolution DAC. This result demonstrates that the RIS can suppress the hardware loss as well.

VI. CONCLUSION AND FUTURE WORKS

The secrecy rate maximization problem for mmWave communications with hardware limitations at the AP and RIS was investigated in this paper. The RIS phase shifts, transmit beamforming vector were jointly optimized to maximize the secrecy rate under the hardware constraint and unit-modulus constraints. To solve this problem, we proposed an AO-based algorithm. Specifically, the transmit beamforming is obtained by using the SCA method, and the RIS phase shift matrix was obtained by using the element-wise BCD method. Finally, numerical results have shown that the proposed AO-based algorithm outperforms conventional schemes in terms of secrecy rate. Moreover, the numerical results also show that when the mmWave system is equipped with RIS, the mmWave system does not need to equip with excessive RF chains and high-resolution ADCs. In this paper, we consider the scenario with a perfect channel. However, the channel is difficult to obtain due to the passive feature of the IRS. Hence, a robust transmission design by assuming an imperfect channel is crucial. In future works, we will design a robust transmission scheme.

APPENDIX A
THE PROOF OF THEOREM 1

We assume ϕ_i as one block of BCD, (28a) can be rewritten as

$$R_s = \left(\frac{|\theta^T \mathbf{c}|^2 + \|\theta^T \mathbf{A}\|^2 + \sigma_c^2}{|\theta^T \mathbf{d}|^2 + \|\theta^T \mathbf{B}\|^2 + \sigma_d^2} \right) \left(\frac{\|\theta^T \mathbf{B}\|^2 + \sigma_d^2}{\|\theta^T \mathbf{A}\|^2 + \sigma_c^2} \right), \quad (35)$$

where

$$\begin{aligned} \mathbf{c} &= \sqrt{1 - \eta_b} \text{diag}(\mathbf{h}^H) \mathbf{G} \mathbf{F}_{RF} \mathbf{w}, \mathbf{d} = \sqrt{1 - \eta_b} \text{diag}(\mathbf{h}_e^H) \mathbf{G} \mathbf{F}_{RF} \mathbf{w} \\ \mathbf{A} &= \frac{P}{N_s} \eta_b (1 - \eta_b) \text{diag}(\mathbf{h}^H) \mathbf{G} \mathbf{F}_{RF} \text{diag}(\mathbf{w}) \\ \mathbf{B} &= \frac{P}{N_s} \eta_b (1 - \eta_b) \text{diag}(\mathbf{h}_e^H) \mathbf{G} \mathbf{F}_{RF} \text{diag}(\mathbf{w}) \end{aligned} \quad (36)$$

To simplify (35), we expand $|\theta^T \mathbf{c}|^2$, $|\theta^T \mathbf{d}|^2$, $|\theta^T \mathbf{A}|^2$, and $|\theta^T \mathbf{B}|^2$ as

$$\begin{aligned} |\theta^T \mathbf{c}|^2 &= |e^{j\phi_i} c_i + p_i|^2 = |c_i|^2 + |p_i|^2 \\ &+ (\text{Re}\{c_i\} \text{Re}\{p_i\} + \text{Im}\{c_i\} \text{Im}\{p_i\}) \cos(\phi_i) \\ &- (\text{Re}\{c_i\} \text{Im}\{p_i\} + \text{Im}\{c_i\} \text{Re}\{p_i\}) \sin(\phi_i), \\ |\theta^T \mathbf{d}|^2 &= |e^{j\phi_i} \bar{c}_i + \bar{p}_i|^2 = |\bar{c}_i|^2 + |\bar{p}_i|^2 \\ &+ (\text{Re}\{\bar{c}_i\} \text{Re}\{\bar{p}_i\} + \text{Im}\{\bar{c}_i\} \text{Im}\{\bar{p}_i\}) \cos(\phi_i) \\ &- (\text{Re}\{\bar{c}_i\} \text{Im}\{\bar{p}_i\} + \text{Im}\{\bar{c}_i\} \text{Re}\{\bar{p}_i\}) \sin(\phi_i), \\ |\theta^T \mathbf{A}|^2 &= \sum_{k=1}^{N_t} |e^{j\phi_i} q_{i,k} + v_k|^2 = \sum_{k=1}^{N_t} |q_{i,k}|^2 + \sum_{k=1}^{N_t} |v_k|^2 \\ &+ \sum_{k=1}^{N_t} (\text{Re}\{q_{i,k}\} \text{Re}\{v_k\} + \text{Im}\{q_{i,k}\} \text{Im}\{v_k\}) \cos(\phi_i) \\ &- \sum_{k=1}^{N_t} (\text{Re}\{q_{i,k}\} \text{Im}\{v_k\} + \text{Im}\{q_{i,k}\} \text{Re}\{v_k\}) \sin(\phi_i), \\ |\theta^T \mathbf{B}|^2 &= \sum_{k=1}^{N_t} |e^{j\phi_i} \bar{q}_{i,k} + \bar{v}_k|^2 = \sum_{k=1}^{N_t} |\bar{q}_{i,k}|^2 + \sum_{k=1}^{N_t} |\bar{v}_k|^2 \\ &+ \sum_{k=1}^{N_t} (\text{Re}\{\bar{q}_{i,k}\} \text{Re}\{\bar{v}_k\} + \text{Im}\{\bar{q}_{i,k}\} \text{Im}\{\bar{v}_k\}) \cos(\phi_i) \\ &- \sum_{k=1}^{N_t} (\text{Re}\{\bar{q}_{i,k}\} \text{Im}\{\bar{v}_k\} + \text{Im}\{\bar{q}_{i,k}\} \text{Re}\{\bar{v}_k\}) \sin(\phi_i), \end{aligned} \quad (37)$$

where

$$\begin{aligned} p_i &= \sum_{j \neq i}^{N_r} e^{j\phi_j} c_j, \bar{p}_i = \sum_{j \neq i}^{N_r} e^{j\phi_j} d_j, \bar{c}_i = d_i, \\ q_{i,k} &= a_{i,k}, \bar{q}_i = b_{i,k} \\ v_k &= \sum_{j \neq 1}^{N_r} e^{j\phi_j} a_{k,j}, \bar{v}_k = \sum_{j \neq 1}^{N_r} e^{j\phi_j} b_{k,j} \end{aligned} \quad (38)$$

We continue to simplify (35) by introducing auxiliary variables μ_i , $\bar{\mu}_i$, η_i , $\bar{\eta}_i$, λ_i , $\bar{\lambda}_i$, ρ_i , and $\bar{\rho}_i$.

$$R_s = \left(\frac{\mu_i + \bar{\mu}_i \cos(\phi_i) - \bar{\mu}_i \sin(\phi_i)}{\eta_i + \bar{\eta}_i \cos(\phi_i) - \bar{\eta}_i \sin(\phi_i)} \right) \left(\frac{\lambda_i + \bar{\lambda}_i \cos(\phi_i) - \bar{\lambda}_i \sin(\phi_i)}{\rho_i + \bar{\rho}_i \cos(\phi_i) - \bar{\rho}_i \sin(\phi_i)} \right), \quad (39)$$

where

$$\begin{aligned} \mu_i &= |c_i|^2 + |p_i|^2 + \sum_{k=1}^{N_t} |q_{i,k}|^2 + \sum_{k=1}^{N_t} |v_k|^2 + \sigma_c^2 \\ \bar{\mu}_i &= (\text{Re}\{c_i\} \text{Re}\{p_i\} + \text{Im}\{c_i\} \text{Im}\{p_i\}) \\ &+ \sum_{k=1}^{N_t} (\text{Re}\{q_{i,k}\} \text{Re}\{v_k\} + \text{Im}\{q_{i,k}\} \text{Im}\{v_k\}) \\ \tilde{\mu}_i &= \sum_{k=1}^{N_t} (\text{Re}\{q_{i,k}\} \text{Im}\{v_k\} + \text{Im}\{q_{i,k}\} \text{Re}\{v_k\}) \\ \eta_i &= |\bar{c}_i|^2 + |\bar{p}_i|^2 + \sum_{k=1}^{N_t} |\bar{q}_{i,k}|^2 + \sum_{k=1}^{N_t} |\bar{v}_k|^2 + \sigma_d^2 \\ \bar{\eta}_i &= (\text{Re}\{\bar{c}_i\} \text{Re}\{\bar{p}_i\} + \text{Im}\{\bar{c}_i\} \text{Im}\{\bar{p}_i\}) \\ &+ \sum_{k=1}^{N_t} (\text{Re}\{\bar{q}_{i,k}\} \text{Re}\{\bar{v}_k\} + \text{Im}\{\bar{q}_{i,k}\} \text{Im}\{\bar{v}_k\}) \\ \tilde{\eta}_i &= \sum_{k=1}^{N_t} (\text{Re}\{\bar{q}_{i,k}\} \text{Im}\{\bar{v}_k\} + \text{Im}\{\bar{q}_{i,k}\} \text{Re}\{\bar{v}_k\}) \\ \rho_i &= \sum_{k=1}^{N_t} |q_{i,k}|^2 + \sum_{k=1}^{N_t} |v_k|^2 + \sigma_c^2 \\ \bar{\rho}_i &= \sum_{k=1}^{N_t} (\text{Re}\{q_{i,k}\} \text{Re}\{v_k\} + \text{Im}\{q_{i,k}\} \text{Im}\{v_k\}) \\ \tilde{\rho}_i &= \sum_{k=1}^{N_t} (\text{Re}\{q_{i,k}\} \text{Im}\{v_k\} + \text{Im}\{q_{i,k}\} \text{Re}\{v_k\}) \\ \lambda_i &= \sum_{k=1}^{N_t} |\bar{q}_{i,k}|^2 + \sum_{k=1}^{N_t} |\bar{v}_k|^2 + \sigma_d^2 \\ \bar{\lambda}_i &= \sum_{k=1}^{N_t} (\text{Re}\{\bar{q}_{i,k}\} \text{Re}\{\bar{v}_k\} + \text{Im}\{\bar{q}_{i,k}\} \text{Im}\{\bar{v}_k\}) \\ \tilde{\lambda}_i &= \sum_{k=1}^{N_t} (\text{Re}\{\bar{q}_{i,k}\} \text{Im}\{\bar{v}_k\} + \text{Im}\{\bar{q}_{i,k}\} \text{Re}\{\bar{v}_k\}) \end{aligned} \quad (40)$$

Let $\tan(\frac{\phi_i}{2}) = t$, we have $\sin(\phi_i) = \frac{2t}{1+t^2}$ and $\cos(\phi_i) = \frac{1-t^2}{1+t^2}$. (39) is rewritten as

$$R_s = \left(\frac{\mu_i(1+t^2) + \bar{\mu}_i(1-t^2) - \tilde{\mu}_i 2t}{\eta_i(1+t^2) + \bar{\eta}_i(1-t^2) - \tilde{\eta}_i 2t} \right) \left(\frac{\lambda_i(1+t^2) + \bar{\lambda}_i(1-t^2) - \tilde{\lambda}_i 2t}{\rho_i(1+t^2) + \bar{\rho}_i(1-t^2) - \tilde{\rho}_i 2t} \right). \quad (41)$$

When the derivative of (41) is 0, the optimal solution ϕ_i^* can be determined by the following equation

$$\frac{(\mu_i - \bar{\mu}_i)t - \tilde{\mu}_i}{\mu_i(1+t^2) + \bar{\mu}_i(1-t^2) - \tilde{\mu}_i 2t} - \frac{(\eta_i - \bar{\eta}_i)t - \tilde{\eta}_i}{\eta_i(1+t^2) + \bar{\eta}_i(1-t^2) - \tilde{\eta}_i 2t} + \frac{(\lambda_i - \bar{\lambda}_i)t - \tilde{\lambda}_i}{\lambda_i(1+t^2) + \bar{\lambda}_i(1-t^2) - \tilde{\lambda}_i 2t} - \frac{(\rho_i - \bar{\rho}_i)t - \tilde{\rho}_i}{\rho_i(1+t^2) + \bar{\rho}_i(1-t^2) - \tilde{\rho}_i 2t} = 0, \quad (42)$$

The (42) can be solved using a one dimension search in [19]. Finally, the **Theorem 1** is proved.

REFERENCES

- [1] M. Di Renzo, A. Zappone, M. Debbah, M.-S. Alouini, C. Yuen, J. de Rosny, and S. Tretyakov, "Smart radio environments empowered by reconfigurable intelligent surfaces: How it works, state of research, and road ahead," arXiv preprint arXiv:2004.09352, 2020
- [2] S. Zhou, W. Xu, K. Wang, M. Di Renzo, and M.-S. Alouini, "Spectral and energy efficiency of IRS-assisted MISO communication with hardware impairments," *IEEE Wireless Commun Lett.*, 2020.
- [3] C. Pan, H. Ren, K. Wang, M. Elkashlan, A. Nallanathan, J. Wang, and L. Hanzo, "Intelligent reflecting surface aided MIMO broadcasting for simultaneous wireless information and power transfer," *IEEE J. Sel. Areas Commun.*, pp. 1–1, 2020
- [4] G. Zhou, C. Pan, H. Ren, K. Wang, M. Di Renzo, and A. Nallanathan, "Robust beamforming design for intelligent reflecting surface aided MISO communication systems," *IEEE Wireless Commun. Lett.*, Early Access, 2020.
- [5] R. Karasik, O. Simeone, M. Di Renzo, and S. Shamai, "Beyond max-SNR: Joint encoding for reconfigurable intelligent surfaces," arXiv preprint arXiv:1911.09443, 2019.
- [6] S. Zhou, W. Xu, K. Wang, M. Di Renzo, and M.-S. Alouini, "Spectral and energy efficiency of IRS-assisted MISO communication with hardware impairments," *IEEE Wireless Commun. Lett.*, Early Access, 2020.
- [7] Shen H, Xu W, Gong S, et al. Secrecy rate maximization for intelligent reflecting surface assisted multi-antenna communications[J]. *IEEE Commun Lett*, vol. 9, no. 23, pp. 1488-1492, Jul.2019.
- [8] Chen J, Liang Y C, Pei Y, et al. Intelligent reflecting surface: A programmable wireless environment for physical layer security[J]. *IEEE Access*, vol. 7, pp. 82599-82612, 2019.
- [9] Lu X, Yang W, Guan X, et al. Robust and Secure Beamforming for Intelligent Reflecting Surface Aided mmWave MISO Systems[J]. arXiv preprint arXiv:2003.11195, 2020.
- [10] Y. Xiu, Y. Zhao, Y. Liu, J. Zhao, O. Yagan, and N. Wei, "IRS-assisted millimeter wave communications: Joint power allocation and beamforming design," arXiv preprint arXiv:2001.07467, 2020
- [11] C. Pradhan, A. Li, L. Song, B. Vucetic, and Y. Li, "Hybrid precoding design for reconfigurable intelligent surface aided mmwave communication systems," *IEEE Wireless Commun. Lett.*, vol. 9, no. 7, pp. 1041–1045, Jul. 2020.
- [12] J. Zhang et al., "Performance analysis of mixed-ADC massive MIMO systems over Rician fading channels," *IEEE J. Sel. Areas Commun.*, vol. 35, no. 6, pp. 1327–1338, Jun. 2017.
- [13] J. Mo et al., "Hybrid architectures with few-bit ADC receivers: Achievable rates and energy-rate tradeoffs," *IEEE Trans. Wireless Commun.*, vol. 16, no. 4, pp. 2274–2287, 2017.
- [14] Zhi K, Pan C, Ren H, et al. "Uplink Achievable Rate of Intelligent Reflecting Surface-Aided Millimeter-Wave Communications with Low-Resolution ADC and Phase Noise," arXiv preprint arXiv:2008.00437, 2020.
- [15] S. Boyd and L. Vandenberghe, *Convex Optimization*. Cambridge university Press, 2004
- [16] Zhi K, Pan C, Ren H, et al. "Uplink Achievable Rate of Intelligent Reflecting Surface-Aided Millimeter-Wave Communications with Low-Resolution ADC and Phase Noise." arXiv preprint arXiv:2008.00437, 2020.
- [17] O. Orhan, E. Erkip, and S. Rangan, "Low power analog-to-digital conversion in millimeter wave systems: Impact of resolution and bandwidth on performance," in *Proc. IEEE ITA*, Feb. 2015, pp. 191–198.
- [18] Q. Wu and R. Zhang, "Intelligent reflecting surface enhanced wireless network: Joint active and passive beamforming design," in *IEEE Global Commun. Conf. (GLOBECOM)*, Abu Dhabi, UAE, Dec. 2018, pp. 1–6.
- [19] Y. Cai, Y. Xu, Q. Shi, B. Champagne, and L. Hanzo, "Robust joint hybrid transceiver design for millimeter wave full-duplex MIMO relay systems," *IEEE Trans. Wireless Commun.*, vol. 18, no. 2, pp. 1199–1215, Feb. 2019.